

PAPER • OPEN ACCESS

Imaging fast neural traffic at fascicular level with electrical impedance tomography: proof of principle in rat sciatic nerve

To cite this article: Kirill Aristovich *et al* 2018 *J. Neural Eng.* **15** 056025

View the [article online](#) for updates and enhancements.

Related content

- [Frequency-dependent characterisation of impedance changes during epileptiform activity in a rat model of epilepsy](#)
Sana Hannan, Mayo Faulkner, Kirill Aristovich *et al.*
- [A method for reconstructing tomographic images of evoked neural activity with electrical impedance tomography using intracranial planar arrays](#)
Kirill Y Aristovich, Gustavo Sato dos Santos, Brett C Packham *et al.*
- [Investigation of potential artefactual changes in measurements of impedance changes during evoked activity: implications to electrical impedance tomography of brain function](#)
Kirill Y Aristovich, Gustavo S Dos Santos and David S Holder

Recent citations

- [Electrode fabrication and interface optimization for imaging of evoked peripheral nervous system activity with electrical impedance tomography \(EIT\)](#)
Christopher A R Chapman *et al*
- [Drive and measurement electrode patterns for electrode impedance tomography \(EIT\) imaging of neural activity in peripheral nerve](#)
J Hope *et al*





IOP | ebooks™

Bringing you innovative digital publishing with leading voices to create your essential collection of books in STEM research.

Start exploring the collection - download the first chapter of every title for free.

Imaging fast neural traffic at fascicular level with electrical impedance tomography: proof of principle in rat sciatic nerve

Kirill Aristovich¹ , Matteo Donegá², Camille Blochet¹, James Avery¹ , Sana Hannan¹ , Daniel J Chew² and David Holder¹

¹ Department of Medical Physics, University College London, Gower Street, London WC1E 6BT, United Kingdom

² Galvani Bioelectronics, Neuromodulation Devices Team, Stevenage, HERTS SG1 2NY, United Kingdom

E-mail: k.aristovich@ucl.ac.uk

Received 14 March 2018, revised 13 July 2018

Accepted for publication 2 August 2018

Published 23 August 2018



Abstract

Objective. Understanding the coding of neural activity in nerve fascicles is a high priority in computational neuroscience, electroceutical autonomic nerve stimulation and functional electrical stimulation for treatment of paraplegia. Unfortunately, it has been little studied as no technique has yet been available to permit imaging of neuronal depolarization within fascicles in peripheral nerve. *Approach.* We report a novel method for achieving this, using a flexible cylindrical multi-electrode cuff placed around nerve and the new medical imaging technique of fast neural electrical impedance tomography (EIT). In the rat sciatic nerve, it was possible to distinguish separate fascicles activated in response to direct electrical stimulation of the posterior tibial and common peroneal nerves. *Main results.* Reconstructed EIT images of fascicular activation corresponded with high spatial accuracy to the appropriate fascicles apparent in histology, as well as the inverse source analysis (ISA) of compound action potentials (CAP). With this method, a temporal resolution of 0.3 ms and spatial resolution of less than 100 μm was achieved. *Significance.* The method presented here is a potential solution for imaging activity within peripheral nerves with high spatial accuracy. It also provides a basis for imaging and selective neuromodulation to be incorporated in a single implantable non-penetrating peri-neural device.

Keywords: imaging, neural traffic, EIT, electroceuticals, cuff electrode

(Some figures may appear in colour only in the online journal)

1. Introduction

There is currently renewed interest in the coding of neural information in the field of computational neuroscience. Mathematical models may be constructed of the information processing of spikes and refined and verified using electrophysiological measures of spiking activity using

multielectrode arrays [1]. Information is transmitted to the central nervous system through peripheral nerves and any complete description thus requires understanding of spike coding in nerve as well as brain [2]. However, this field is not well developed, which may be attributed to limitations in technology for recording such neural activity within nerves. The anatomical basis for localisation of function in peripheral nerve is not clear. It is well established that peripheral nerves in larger mammals are organised into fascicles apparent on light microscopy but their functional anatomy is poorly understood.



Original content from this work may be used under the terms of the [Creative Commons Attribution 3.0 licence](https://creativecommons.org/licenses/by/3.0/). Any further distribution of this work must maintain attribution to the author(s) and the title of the work, journal citation and DOI.

Historically, the main approach has been the painstaking analysis of multiple serial sections which has permitted identification of somatotopic organisation in the principal human limb nerves [3, 4]. In approximately the distal third of the peripheral nerve, fascicles are generally devoted to a single muscle or receptive field. In about the middle third of the nerve they may merge with other fascicles to form a mixed fascicle, but retain their unique localised somatotopic organisation within the mixed fascicle. The functional organisation of nerves as they rearrange in proximal brachial and lumbosacral plexuses and autonomic nerves is almost entirely unknown. Methods are available to add to this knowledge. Neural tracers may be used to label end organs and their supplying nerves but have been mainly used to trace connections to the CNS [5]. Computerised tracing may be applied to multiple serial histological sections but is time consuming and has only been limited to relatively short lengths of nerve [6]. These two techniques permit identification of anatomical organisation of fascicles but not their functional activity. This has been extensively studied using microelectrodes or, more recently, multielectrode arrays which are linear or 2D [7–10]. However, these only provide a limited subset of spiking activity from the several thousand axons present in most peripheral nerves, according to the chance apposition of the recording contacts. There are also concerns regarding their chronic applications as the presence of rigid foreign material in nerves causes tissue damage and an inflammatory response [11, 12].

There is therefore a pressing need for a novel method which could record functional activity in nerves with the temporal resolution of the compound action potential (CAP), i.e. milliseconds, but be non-penetrating so that it could be left *in situ* over months and produce images of such activity in nerve fascicles chronically. This would permit identification of the localisation of function in peripheral nerve but also yield images of the envelopes of spiking activity which could provide a key to unlocking the neural code in nerve before it arrives in the CNS. It could also have practical application in reconstructive surgery of peripheral nerve after trauma, where it could be used to identify fascicle function and human robotics based on activity in extant peripheral nerve after trauma [13–15]. Further in the field of ‘electroceutical’ stimulation of autonomic nerve for treatment of disease, it could be used to identify the function of fascicles within autonomic nerve and so avoid off-target effects [16, 17]. In this work, we present such a method for the first time.

1.1. Background

1.1.1. Introduction to fast neural electrical impedance tomography (EIT).

Electrical impedance tomography (EIT) is an emerging medical imaging method in which small changes in impedance of a conductive volume may be imaged with an array of external electrodes. It may be used to produce images of neuronal depolarisation over milliseconds, related to small decreases in bulk tissue resistance which occur as ion channels open. This requires averaging over some tens of seconds or minutes in response to repeated evoked activity, but delivers a final data set with images every millisecond of neuronal

depolarisation in the field of interest. We have extended its use to imaging the CAP in peripheral nerve using a non-penetrating soft rubber external nerve cuff with 16–32 electrodes (16 were used in this study as a proof of concept, 32 is currently being investigated). It yields images of CAP volleys with fascicles in the nerve with a resolution of <0.3 ms and ~ 100 μm in the studied rat sciatic nerve. This provides a new technique which could be used to unlock the functional anatomy and envelope of spike coding in somatic and autonomic nerve and support the study of neural coding in peripheral nerve in the future. Mathematically, EIT is close to inverse source localisation. However, the method has significant advantages: orders of magnitude more independent data (for N electrodes there are $O(N^2)$ independent measurements at a time compared to $O(N)$ for ISA), a potentially unique solution, no field cancellation problem, and no theoretical limitations on the accuracy [18–20]. In this work, the resolution with 16 circumferential electrodes was 100 μm . As it is a proof of principle, we elected to demonstrate this in the two major fascicles in the sciatic nerve. However, the resolution could in the future be increased with larger numbers of electrodes. With 32 electrodes, modelling suggests that a resolution of 30 μm could be achieved in rat sciatic nerve. This would be at the sub-fascicular level and close to imaging small groups of axons, depending on the axon diameter. Thus the technique potentially is not limited to the fascicle-level, but could also be used to image much smaller axonal-level activity with an increased number of electrodes.

In this implementation multiple transfer impedances were rapidly recorded using an external cylindrical electrode array (figure 1). Each measurement was made by the injection of a constant current ($30\mu\text{A}$ at 6kHz) through a pair of electrodes placed 5 electrodes apart (135° , according to the optimal distinguishability/SNR [20]) with simultaneous measurements of the corresponding voltage changes on the 14 remaining electrodes. Impedance changes were measured as the bulk resistance of active nerve fibres decreases by c. 0.1% during the opening of ion channels during the action potential; this allows the applied current to pass into the intracellular space. During the EIT measurement, current was sequentially applied to all possible electrode pairs, yielding 234 (14×16) transfer impedances. These impedances were then reconstructed into tomographic images every 0.33 ms using a cylindrical finite element mesh through regularization and inversion of a Jacobian matrix which relates conductivity of image voxels to the boundary voltage measurements. EIT is a soft-field problem and image spatial resolution is typically about 10% of the image diameter. Reproducible and biophysically plausible fast neural impedance changes have been recorded in crab nerves *ex vivo* [21–24]. Fast neural EIT images have been obtained in rat cerebral cortex during normal [25, 26] and epileptic [27] activity, with a temporal resolution of <3 ms, and spatial resolution of less than 200 μm , using arrays of epicortical electrodes.

The rat sciatic nerve has been selected as a suitable model for studying the feasibility and current limitations of EIT imaging in a peripheral nerve as it has a reasonably large diameter of about 1.5 mm and a well delineated internal

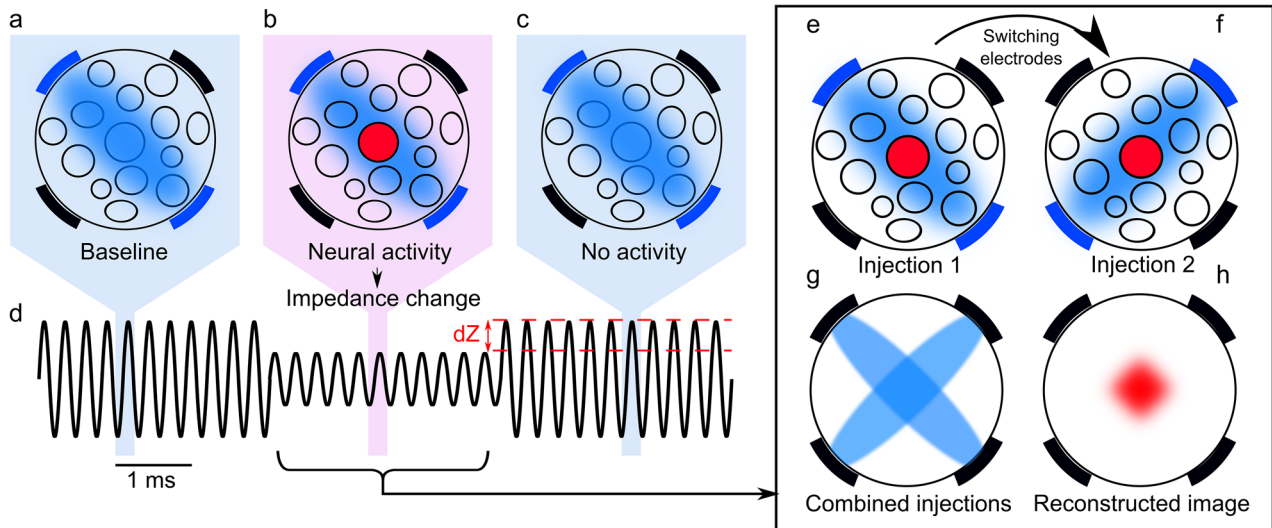


Figure 1. The principle of fast neural EIT in a ‘model’ peripheral nerve. (a)–(d) The impedance change occurs during neural activity (b) with respect to the background (a) and (c), which is measured by passing a constant current through a pair of external peri-neural electrodes, and recording the voltage response on the remaining electrodes (d). Currently used cuffs have 16–32 electrodes; just 4 are shown here for explanatory purposes. (e) and (f) The pair is then switched from one to another and the paradigm is repeated covering all possible electrode combinations. (g) These measured transfer impedances can be reconstructed into tomographic images using principles similar to x-ray back projection. (h) Reconstructed images of the neural activity have a resolution of less than 100 μm and 0.3 ms with current methods using 6 kHz applied current and 16 electrodes in a nerve 1.5 mm in diameter.

fascicular organization [28]. The proximal and mid part of the nerve comprises 4 histologically distinguishable fascicles which divide distally into the tibial, common peroneal, posterior cutaneous, and sural nerves, and express distinct architecture for motor and sensory function [28, 29]. Mixed sensory orthodromic and motor antidromic CAPs were produced by electrical stimulation of the common peroneal or posterior tibial nerves. This produced the largest possible fibre activation and at the same time allowed improvement of the SNR by triggered ensemble averaging [26].

1.1.2. Comparison with inverse source analysis (ISA) of the CAP. Inverse source modelling of physiological endogenous activity is a mature field which has been extensively applied to brain function recorded by EEG and MEG. Recently, interest has developed in its application to imaging fascicular activity in nerve [30]. Although the inverse problem is similar in both EIT and inverse source modelling, EIT has the advantage that the electric source is known. There is, therefore, a unique inverse solution in principle in contrast to inverse source imaging, which does not have a unique solution and requires simplifying assumptions of uncertain validity. In addition, more independent measures are obtained for the same number of electrodes in EIT: for n electrodes there are $O(N^2)$ independent measurements at a time, compared to $O(N)$ for ISA). In addition, whereas ISA is limited as positive and negative fields may cancel without reaching surface electrodes, impedance changes due to ion channel opening are highly unimodal and so any cancellation of signals with EIT is negligible [18, 31, 32]. However, EIT in its current configuration for imaging fast neural activity in the brain requires several minutes of averaging to a repeated trigger whereas the SNR of ratio of local field potential recordings is higher and permits real-time signal classification.

Early efforts using Loreta algorithms had limited success. With 56 longitudinal electrodes around the rat sciatic nerve, activity in multiple pathways could only be successfully localised in 25% of cases [33]. Since 2011, there have been significant advances in this methodology, mainly in conjunction with the FINE neural cuff electrode [34] which has a geometry of two planes of eight electrodes which constrain the nerve into a rectangular cross-section. In several studies with gradually improving algorithms based on beamforming and Bayesian signal training approaches, it has been shown that activity of the tibial and peroneal fascicles in the main sciatic trunk may be identified in the rabbit acutely and dog in chronic preparations. The algorithms may be used to generate images; modelling and tank studies suggested a localisation accuracy of c. 1 mm using the FINE electrodes with 16 contacts around the dog sciatic nerve [30, 35, 36]. The methods have been shown to recover movement intent in real time with an SNR of 1.5–2.5 (3–7 dB) and accuracy of 70%–80% in freely moving animals. In individual examples, reconstructed sources can be shown to correlate with the histological location of the tibial and peroneal fascicles. However, the repeatability across studies is not clear; in [37], reconstructed source locations were overlaid on histology in three of the seven nerves studied. Of the six fascicles represented, one was completely off, and three were largely outside the histological fascicle. For single fascicle activity, the algorithms were rapid and able to deliver localisation in almost real-time over milliseconds. However, for more realistic combined physiological activity with stimulated activity in both fascicles, averaging was needed to produce source discrimination [38].

1.1.3. Experimental design. Here, we report the design and application of imaging axonal traffic in the sciatic nerve of anesthetized rats with EIT using an external cylindrical cuff wrapped

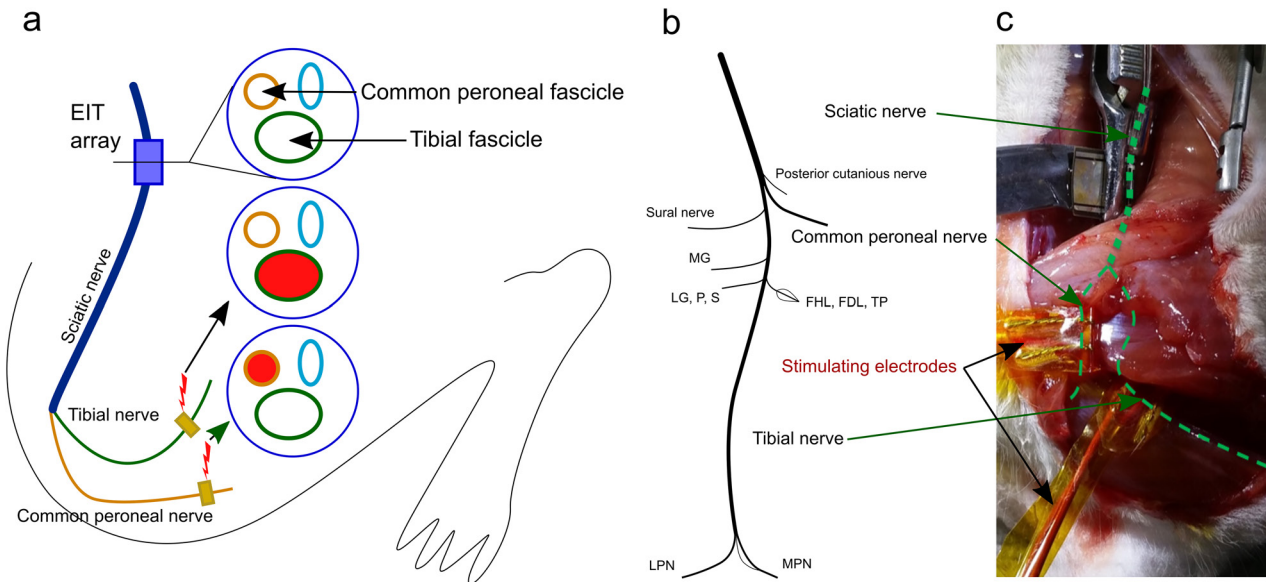


Figure 2. Experimental design and setup. (a) The EIT array was placed on the main sciatic nerve running in the posterior compartment of the thigh approximately 20 mm distal to the greater sciatic foramen. (b) and (c) Two stimulating electrode pairs were placed on the tibial and common peroneal nerves. EIT images were recorded during the repeated activity in the sciatic nerve evoked with 5 Hz stimulation of each branch at a time.

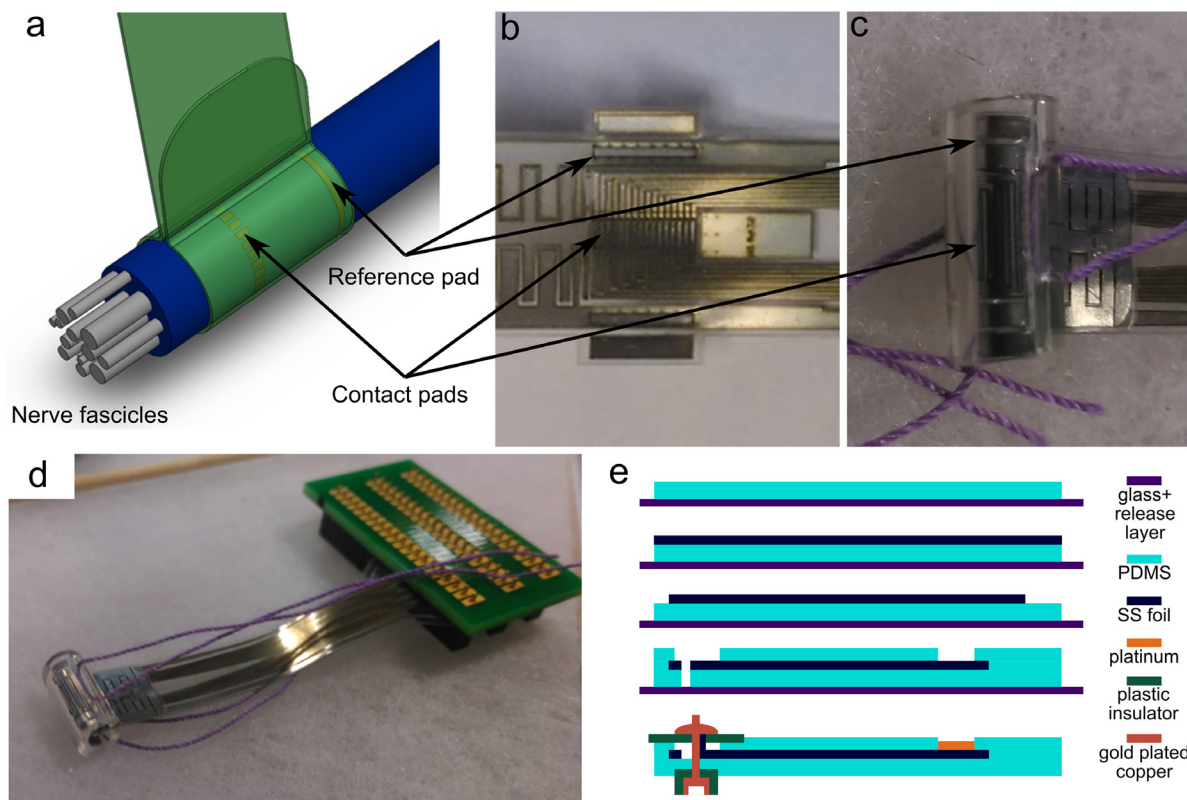


Figure 3. (a) EIT electrode array comprising 16 contacts around the nerve circumference and 2 reference pads located proximally and distally. (b) Electrodes were fabricated as a flat sandwich silicone/stainless steel/silicone structure and (c) were glued onto the inner side of a 1.8 mm I.D. silicone tube to form a 1.4 mm I.D. cuff. (d) The cuff was wired using a custom-made pin-through connector. (e) The detailed fabrication process is explained in text and schematically illustrated here.

around the nerve. Initially we demonstrate the feasibility of measuring impedance signals in the nerve and determine the optimal current frequency for undertaking EIT on the basis of the SNR in single channel recordings. Then we characterize the impedance signal in the myelinated sciatic nerve and demonstrate EIT

imaging of localized, spatially separated neural activity in sciatic nerve evoked by electrical stimulation of the distal tibial and common peroneal branches (figure 2). Finally, we cross-validate EIT images against histological cross-sections of the sciatic nerve obtained with the cuff in place as well as inverse source

imaging of the recorded CAP. The accuracy of EIT was compared to that of ISA. There have been recent significant advances in ISA, which include hybrid Bayesian signal extraction (HBSE) [35] and other forms of signal-matched filtering. We have not yet implemented such approaches for fast neural nerve EIT, as satisfactory imaging has been possible without them. We therefore selected the standard Lead-field approach in combination with Tikhonov regularisation [39]. This allowed head-to-head comparison between the techniques as mathematically inverse problems are solved identically and the only difference is in the physics and acquired data.

2. Methods

2.1. Electrode design

EIT was performed using flexible cuff electrode arrays made from laser cut stainless-steel foil, 12.5 μm thick, on silicone rubber. Arrays comprised 16 0.15×0.7 mm electrode contacts, each spaced 0.15 mm apart (figure 3). Connecting tracks were 150 μm wide with an inter-track spacing of 35 μm . The total thickness of the array was 220 to 250 μm . After fabrication, electrodes were platinized to reduce contact impedance below 1 k Ω at 10 Hz for each electrode. This reduced noise from the electrode–electrolyte interface by about two orders of magnitude.

The electrodes were fabricated using a laser-cutting technique with the following protocol: (1) The 10 μm release layer (Poly(4-Styrenesulfonic Acid), Sigma Aldrich, UK) was spin-coated on the 70×40 mm glass slides (Fisher Scientific, UK) followed by 100 μm layer of the silicone rubber (MED4-4220, Polymer Systems Technology Ltd, US). (2) The rubber was cured for 5 min at 100 deg C in the oven. (3) Stainless steel foil (0.0125 mm, Advent Research Materials, UK) was glued on top of the rubber. (4) The electrode profile was cut using 20 W precision laser cutter (355 nm, IDG lab, UCL, UK). (5) Excess foil was peeled off, and the second 100 μm layer of the silicone rubber spin-coated on top. (6) The electrode openings and connector pads were laser-cut and peeled away. (7) Finally, the array was glued on the inside of the 1.8 mm ID silicone rubber tube (Tygon LMT-55, Fisher scientific, UK) with thread mounted to assist implantation, and connector side was attached to a custom PCB using 20-way 1.5 mm connectors (Farnell, UK).

2.2. Animals

All animal work undertaken in this study were approved by the UK Home Office and in accordance with its regulations (Project number: PPL 70/7450). A total of 8 Sprague-Dawley adult male rats weighing 300–450 g were used for recordings. Anaesthesia was induced with a 5% isoflurane in 100% O₂. Rats were then intubated using a small animal laryngoscope [40] and an 18 G cannula and mechanical ventilation was provided, using a Harvard Apparatus Inspira Ventilator (Harvard Apparatus, Ltd, UK), with a 50/50% gas mixture of O₂ and air. Arterial and venous access was established through cannulation (BD Insite/Vialon, Becton, Dickinson U.K. Ltd)

of the right femoral vessels. The arterial blood pressure was monitored (Cardiicap 5, Datex Ohmeda) and the mean arterial pressure (MAP) kept between 90 and 110 mmHg using labetalol and adrenaline as necessary. Once intravenous access had been established, a constant infusion of propofol was initiated. Access to the left sciatic nerve was performed by splitting the biceps femoris and vastus lateralis by inserting a retractor. Access to the posterior tibial nerve was established through splitting tibialis anterior and extensor digitorum long. Access to the common peroneal nerve was established through a 2 mm lateral incision in biceps femoris near the knee joint. After that the retainers were removed, and internal cavities were closed with cotton soaked in 0.9% sterile saline solution. Procedures were performed on a vibration isolated table (Thorlabs Inc., USA) and, throughout experiments, the core body temperature of the rat was controlled with a homeothermic heating unit (Harvard Apparatus, Kent, UK) and maintained at 37 °C. All surgical procedures were performed using aseptic techniques.

2.3. Electric stimulation

For all studies, a square biphasic (positive first) constant current temporal waveform was delivered using a balanced current source (Keithley, UK model no 6221) with 5 mA amplitude, 200 μs pulse width, 2 Hz frequency (500 ms inter-stimulus time) for impedance characterisation and 1–3 mA amplitude, 50 μs pulse width, 5 Hz frequency (200 ms inter-stimulus time) for stimulation of branches. The waveform was delivered using bipolar Ag hook electrodes.

2.4. Impedance measurement

The EIT cuff was placed on the main trunk of the sciatic nerve running in the posterior compartment of the thigh approximately 20 mm distal to the greater sciatic foramen in anaesthetized rats (figure 4(a)). Transfer impedances were recorded by injecting constant current of 30 μA peak to peak at 6000 Hz (5 nC/phase) using a commercial current source (Keithley, UK model no 6221). Each current injection was performed through a single pair of electrodes with a spacing of 5 intervening electrodes, selected using a custom made multiplexer [41]. The electrode spacing was based on the best depth distinguishability, ensuring enough current would penetrate inside the nerve without compromising resolution [42]. The resulting voltages were recorded with the remaining 14 electrodes with respect to the reference ring electrode using a commercial high-specification ActiChamp EEG amplifier (BrainProducts GmbH, Germany) with a sampling rate of 100 kHz at 24 bits per channel (figure 4(b)). Each transfer impedance measurement current injection was averaged over 150 consecutive 200 ms trials lasting 30 s. This yielded a total of 234 (16×14) transfer impedances averaged over an 8 min window. Impedance changes were then demodulated with a ± 3000 Hz bandwidth around the carrier frequency, giving 0.3 ms time resolution within the 200 ms trials (figure 4(c)).

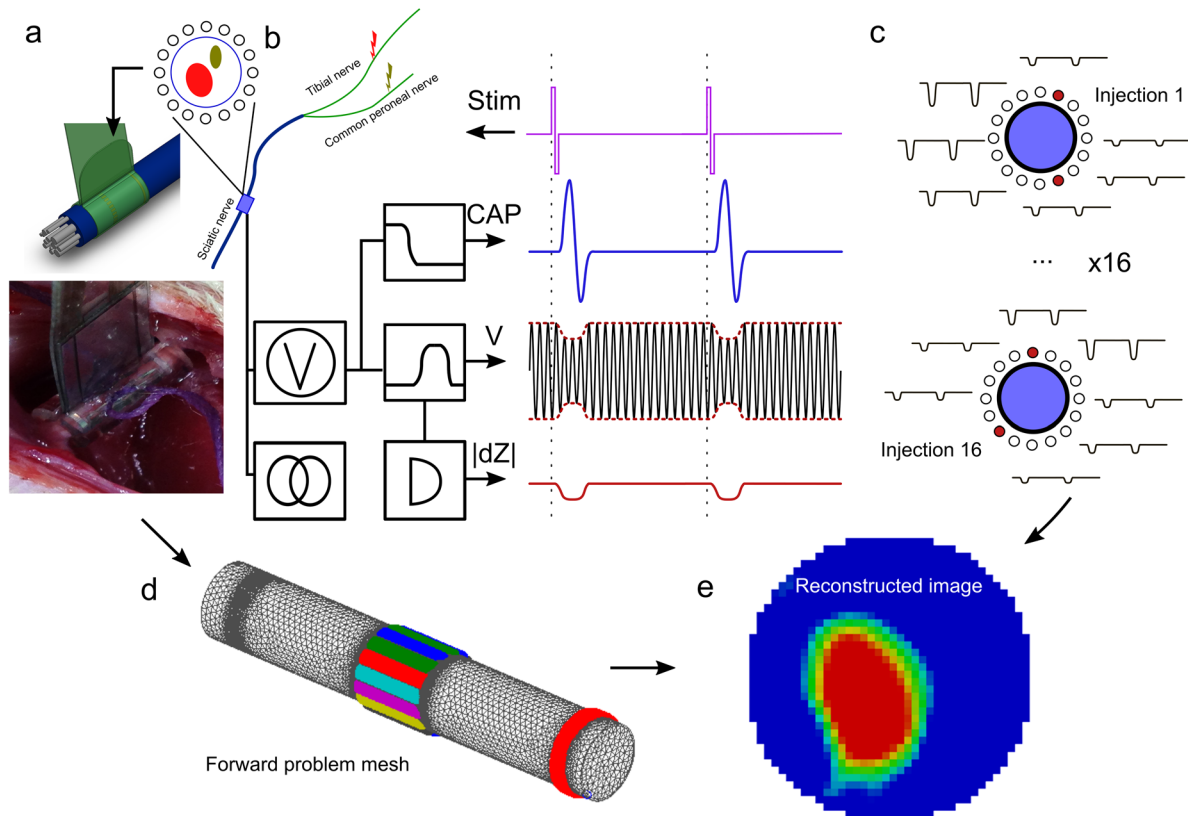


Figure 4. EIT data collection and processing. (a) The 16 electrode array cuff was placed around the exposed sciatic nerve. Two bipolar stimulation electrode cuffs were placed over the exposed tibial and common peroneal nerves respectively. (b) The tibial or peroneal nerves were electrically stimulated with biphasic pulses (Stim) and 100 cycles averaged for each impedance measurement. Simultaneously a constant amplitude current of $30 \mu\text{A}$ at 6 kHz was injected through selected pairs of electrodes. The resulting voltages were recorded on all other 14 electrodes with respect to a reference in distal circumferential electrode. The voltages were then low pass filtered at 2 kHz to yield evoked CAP, and band pass filtered at $6 \pm 3 \text{ kHz}$ to yield an amplitude modulated sine wave (V), which was demodulated to reveal the impedance change ($|dZ|$). (c) This sequence was repeated for all 16 electrode injection pairs. Two injection pairs are illustrated. Red— injection pair; hollow—recording electrodes; black traces—resulting impedance decreases. (d) Images were reconstructed using a 2×10^6 -element FEM tetrahedral, and 100 000-element hexahedral meshes with electrode locations taken from the histology. (e) The resulting data were stored in a 4D spatiotemporal format.

2.5. EIT imaging

EIT images were reconstructed using the following procedure, described in detail in [43], with all of the used tools available online (<https://github.com/EIT-team/>).

(1) Forward problem solution. The model of the nerve was chosen to be cylindrical, with diameter determined from histological slices for each individual nerve by fitting the circle (best linear fit). The electrode locations in the forward model were co-registered with histological slices by fitting the circular profile to the histological image and manual evaluation of the sites of the beginning and the end of the cuff array. As histological images of the cuff were distorted during preparation (the electrode cuff opened and buckled), the recording placement was corrected by second order deformation of the shape determined by the histology to the circular profile which was fitted as a nerve domain. The procedure was justified by the observations made during the recording that all of the electrodes were in good contact with the nerve and cuff shape was almost perfectly cylindrical. For the nerves where histology was not available, the generic mesh (1.4 mm diameter) and electrode locations (equally

spaced around the circumference) were used (figure 4(d)). The forward problem was solved using a complete electrode model utilizing the UCL PEIT forward solver [44]. Forward solution provided a linearized conductivity- $|dZ|$ matrix, which was projected onto regular 100 k-element hexahedral mesh for imaging [43].

(2) Inverse problem. Jacobian matrix inversion was accomplished using 0th order Tikhonov regularization and post-processed with noised-based voxel correction [43]. The raw $|dZ|$ data at each time frame was reconstructed in first 5 ms after the stimulus resulting in 500 3D images 0.01 ms apart. Background inter-stimulus noise was also projected into volume using the same reconstruction parameters. Then each voxel in each time frame was divided by the standard deviation of the projected noise, resulting in the z -score of the conductivity change with respect to the background noise (figure 4(e)).

2.6. Inverse source analysis (ISA)

The analysis was performed using the CAP recorded simultaneously with EIT. The CAPs were extracted by low-pass filtering (5th order Butterworth filter with 2000 Hz cut-off) and

trial-by-trial averaging of the data, resulting in 16 CAP traces over 200 ms for each dataset. The CAPs were re-referenced to the mean of all channels to get rid of common signal. Then the following was performed: (1) The forward problem was solved using a lead-field matrix approach, linearizing the relationship between inner current density and measured voltages. It was computed with the adjoint fields theorem and electrical reciprocity principle [45] on the exact tetrahedral meshes for each nerve as for EIT. (2) Imaging algorithm (ISA). CAPs were reconstructed into images by lead-field matrix inversion with zeroth order Tikhonov regularisation and noise-based image post-processing using the same technical method and hexahedral meshes as for EIT. The resulting imaging sets were current density amplitude z-score with respect to the background noise.

2.7. Histology

At the end of the experiment, the rats were euthanized and the EIT cuff containing the portion of sciatic nerve was carefully dissected to maintain the correct orientation and alignment. The collected tissues were then embedded in optimal cutting temperature compound (OCT, Tissue-Tek) and immediately frozen on dry ice. Samples were then stored at -20°C . Coronal sections of $30\ \mu\text{m}$ thickness were obtained with a cryostat (Leica Biosystems, CM1950), collected on SuperFrost Plus slides (Fisher Scientific, 10149870) and imaged using a microscope mounted camera. Sections showing the sciatic nerve and the silicone backbone of the EIT cuff were then used to determine the match between the EIT reconstructed images and the spatial distribution of the tibial and common peroneal nerves within the cuff.

2.8. Controls

The following controls were performed in some rats in order to evaluate if the impedance change signals obtained in the recordings were due to genuine impedance changes related to the opening of ion channels rather than artefact: (1) Current amplitude control. The amplitude of the EIT current was varied between 10 and $170\ \mu\text{A}$ in order to ensure if there was proportionality of the impedance signal to the applied current amplitude. This was undertaken in order to ensure the impedance voltage signal conformed to Ohm's Law, and so that the applied current did not itself open ion channels and cause artefactual impedance changes. (2) Current phase control. The phase of the applied current with respect to stimulator was randomized in every trial. (3) No stimulation control. EIT was performed without stimulation to ensure absence of the signal. (4) Stimulation amplitude control. The stimulator amplitude was normally set to the minimal sufficient to cause maximal CAP for the recordings. In this control, the amplitude was increased $5\times$ times in order to ensure the impedance changes are not related to the stimulation artefacts. (5) Stimulation polarity control. The polarity of the stimulation was changed in order to ensure impedance changes were not related to stimulation artefact. (6) Crushed nerve control. The nerve was crushed

after the experiment in order to ensure absence of CAP and impedance changes and exclude all possible artefacts not related to neural activity. (7) Neuromuscular blockade (NMBA) control. NMBA was introduced in order to ensure absence of muscle artefacts.

2.9. Statistical analysis

All results are presented as mean ± 1 SE unless otherwise stated. For each result, the total number of acquired parameters/datasets (n) acquired across number of rats (N). A two-sided paired t -test with respect to background inter-stimulus noise was performed to determine the statistical significance of time-varying changes with P values displayed, unless otherwise stated. All datasets were considered to be independent (i.e. assumed $N * n$ independent cases), even if they came from the same test animal under the NULL hypothesis that peak evoked activity was from the same distribution as background non-evoked activity. Correction was not used since the events (background VS activity) were sufficiently separated in time ($>100\text{ ms}$) for any acquisition/signal processing/filtering to have an effect. One-way ANOVA analysis were performed for variable statistics, such as current amplitude, phase, and polarity controls. For all image comparison statistics Bonferroni correction was used as the separate pixels in the image were correlated by the nature of image reconstruction routine.

3. Results

3.1. Characteristics of impedance changes during the CAP

To establish feasibility of impedance measurement in peripheral nerves and characterize the signal in myelinated nerves, the hind paw was electrically stimulated supramaximally in order to produce a CAP in the sciatic nerve. For single channel impedance recordings, electrical stimulation was produced in the left hind paw between toes 1–2, and 4–5, to ensure stimulation of the entire paw (5 mA, $200\ \mu\text{s}$ pulse width, 2 Hz stimulation). Reproducible single-channel impedance changes had maximum amplitudes of $0.2\% \pm 0.05\%$ (across all significant frequencies, $P < 0.0001$, paired t -test with respect to inter-stimulus noise, $n = 256$, $N = 4$), an average onset of $1.03 \pm 0.01\text{ ms}$ (mean ± 1 SE), and duration of $1.01 \pm 0.04\text{ ms}$. Based on the duration and onset of the EIT signal, significant changes were caused by A or B-fibre activity with conduction velocities between $20\text{--}60\text{ m s}^{-1}$.

The SNR of the evoked averaged peak impedance signal was 8.0 ± 0.3 at 6 kHz ($n = 32$, $N = 4$) at a maximum, corresponding to a single-shot real-time SNR of 0.80 ± 0.03 . It decreased to 2.2 ± 1.0 and 4.0 ± 2.1 at 8 and 10 kHz respectively ($n = 8$, $N = 4$) before increasing to 7.1 ± 3.1 and 5.4 ± 3.0 at 11 and 15 kHz ($n = 8$, $N = 4$). In order to determine if the unexpected non-monotonic decline with frequency was due to noise contamination, the background noise was analysed at different frequencies. The root-mean-square noise $0.5 \pm 0.01\ \mu\text{V}$ at all frequencies except for 8 and 10 kHz where it was $2.5\ \mu\text{V} \pm 0.1\ \mu\text{V}$.

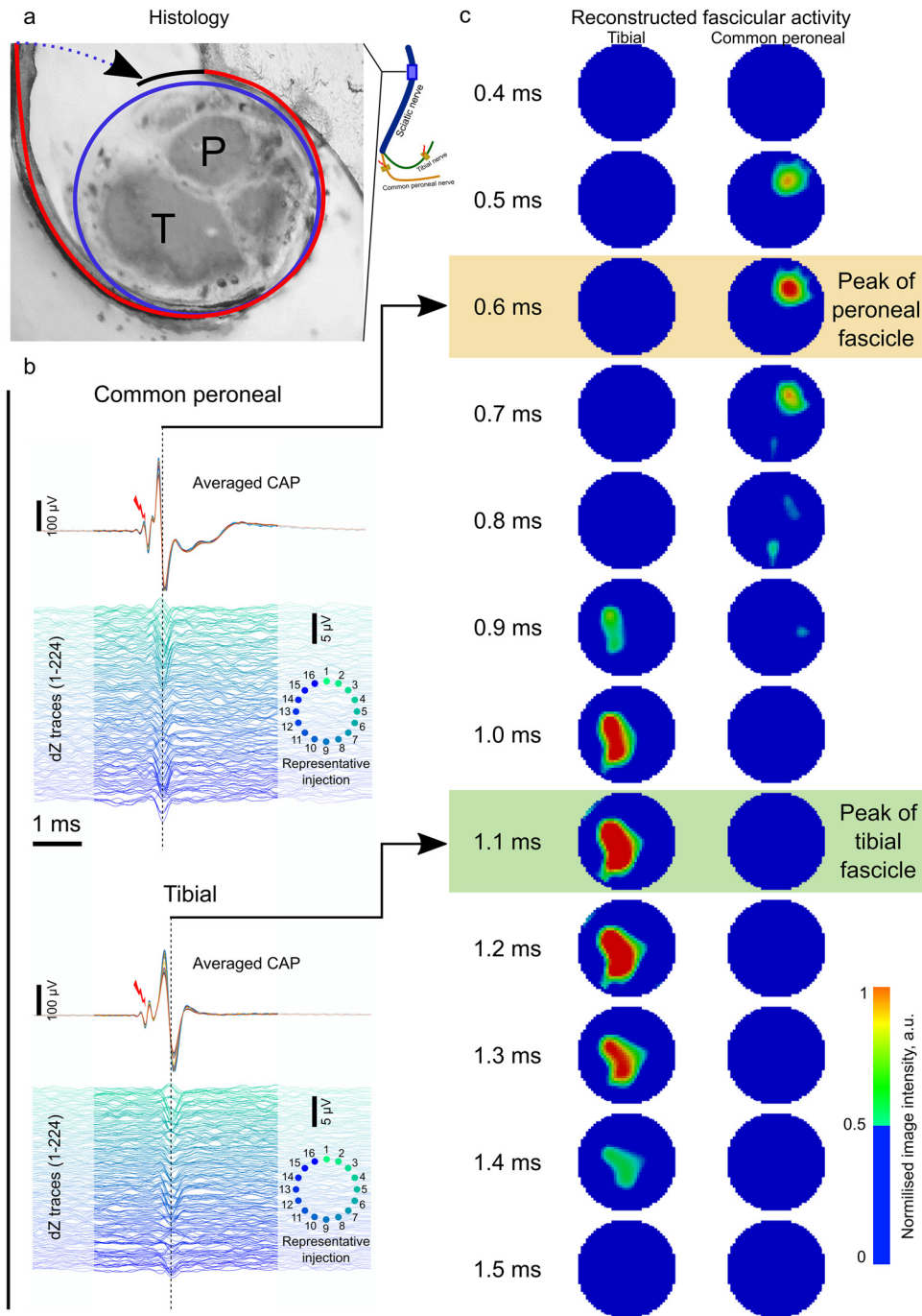


Figure 5. Example of EIT image dataset. (a) The histology image, showing the position of the electrode and tibial and peroneal fascicles. After freeze drying and fixation, the electrode cuff opened—its appearance in the histology image is denoted by the red line. During recording, it was in close contact with the nerve and this is denoted by the blue line, which was used for image reconstruction. (b) Evoked CAP (top) and corresponding impedance changes (lower traces) recorded during to stimulation of the tibial and common peroneal branches. (c) EIT images following common peroneal nerve stimulation (right) and tibial nerve stimulation (left) at different time points (0.4–1.5 ms).

3.2. EIT imaging of functionally distinct fascicles in peripheral nerves

For imaging studies, the tibial and common peroneal nerves were electrically stimulated one at a time using Ag wire hook electrodes, 0.5 mm in diameter; this evoked CAPs in corresponding fascicles within the sciatic nerve (figure 2(a)). A 16-electrode EIT array was placed around the sciatic nerve in the thigh (figure 2(c)). Evoked responses were induced

using supramaximal electrical stimulation with a 50 μs pulse width and 1–3 mA amplitude. Each branch was stimulated repeatedly at 5 Hz with a 200 ms inter-stimulus interval. The stimulator also generated a trigger signal which was used to separate the trials.

The imaging data was collected in seven rats. In three rats the nerves were extracted with the electrode array post-experiment. In these rats the nerve diameter and electrode locations

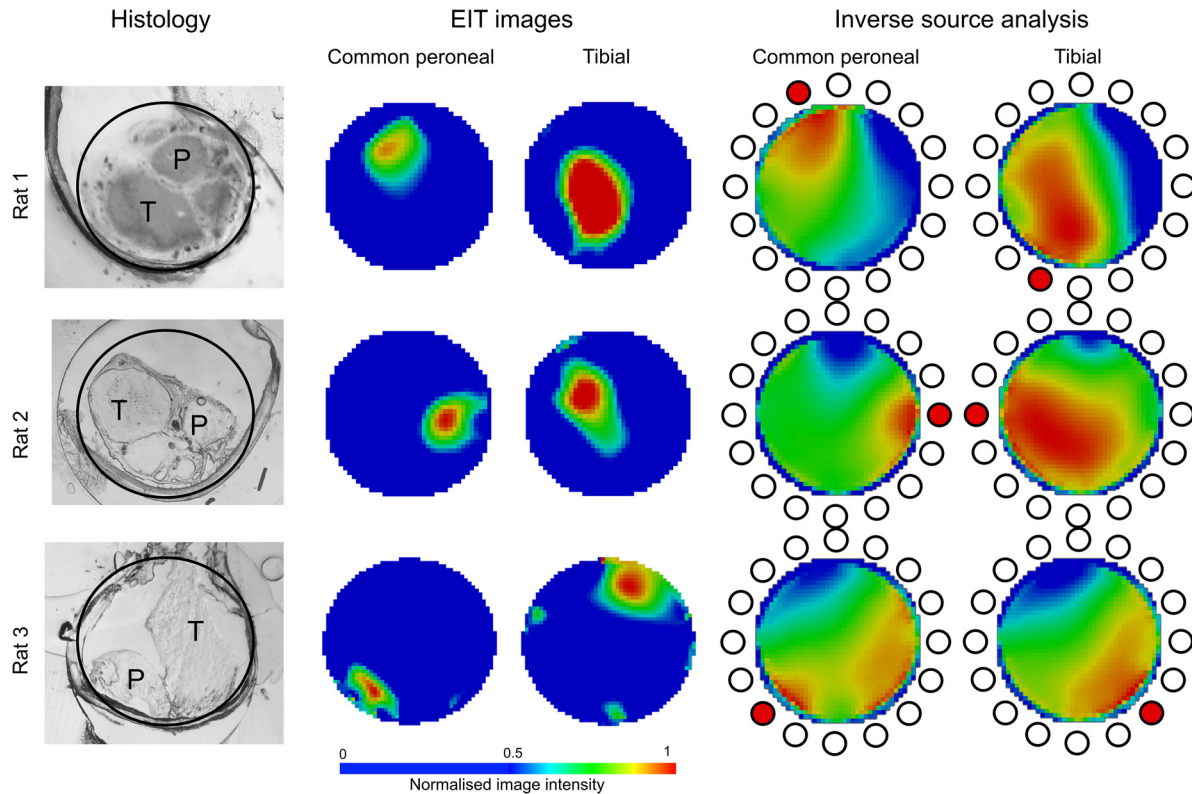


Figure 6. EIT images of the sciatic nerve overlap with morphological localization of tibial and peroneal fascicles. Comparison of the histology (left column, Common peroneal fascicle is marked *P*, tibial fascicle is marked *T*) with EIT images (middle, mean over four sets) and ISA over CAP distribution on the electrodes (left, red filled circle is the location of the electrode on which the largest CAP amplitude was measured).

were obtained for each nerve using histomorphometry. In each rat, four imaging datasets were collected for each branch stimulation, resulting in 56 imaging datasets altogether; 24 of which (in three rats) were used for independent validation of EIT. The resulting average CAP amplitudes measured with the cuff were $250 \pm 50 \mu\text{V}$ and $160 \pm 40 \mu\text{V}$ in response for tibial and peroneal branches stimulation, respectively.

Reproducible localized impedance changes were apparent in the EIT images which correlated visually with the anatomical distribution of the common peroneal and tibial fascicles ($n = 56$ in $N = 7$ rats). These corresponded to stimulation of the tibial (peak at 1.03 ± 0.04 ms, mean ± 1 SE), and peroneal (peak at 0.71 ± 0.02 ms) branches (figure 5).

There were significant regions of activity ($P < 0.005$, two-sided paired *t*-test with respect to background noise), which were spatially separable for tibial and common peroneal branches respectively ($P < 0.001$, $n = 56$ in $N = 7$ rats, two-sided *t*-test with Bonferroni correction). The centres of activity produced by stimulation of single peripheral branch were located in close proximity to each other across the animals for both tibial and peroneal stimulation respectively (all distances were < 0.06 mm, $n = 56$ in $N = 7$ rats). The mean separated volume (non-overlapping region in % of a total volume) was 90% with peroneal and 85% with tibial fascicles. The total mean overlap was $< 15\%$ ($n = 56$ in $N = 7$ rats).

Independent validation of EIT images was performed in three animals by direct comparison with co-registered histological images and ISA of peak CAP activity. ISA was

performed with linear lead field matrix approach using the same meshes and regularisation paradigms as for EIT to make it comparable (see online methods for details). Co-registration of the electrodes on the histological images was performed by fitting the circle to the shape of the cuff and determining the positions of the first and last electrode with respect to the top (figure 5(a)). Comparison showed the position mismatch was $0.1 \text{ mm} \pm 0.03 \text{ mm}$ between EIT and histology, and $0.14 \text{ mm} \pm 0.06 \text{ mm}$ between EIT and inverse source imaging ($n = 24$ in $N = 3$ rats, figure 6).

3.3. Controls

Impedance changes successfully passed all controls in six rats (three rats for controls were used from imaging data set): $n = 12$ for current level control ($P > 0.5$, one-way ANOVA), 360 for current phase ($P > 0.5$, one-way ANOVA), eight for stimulation amplitude and polarity ($P > 0.5$, one-way ANOVA), 360 for NMBA ($P > 0.5$, paired two-sided *t*-test), five for crushed nerve ($P > 0.5$, paired two-sided *t*-test), three for no stimulation ($P > 0.05$, one-side unpaired *t*-test, activity in the expected time frame was compared to inter-stimulus time frame). Injected current with magnitudes lower than $150 \mu\text{A}$ at 6 kHz did not alter the CAP and impedance changes significantly ($P > 0.5$, one-way ANOVA). At higher magnitudes CAP and impedance changes were significantly modified ($p < 0.05$, two-sided paired *t*-test). At magnitudes $> 170 \mu\text{A}$, significant leg movement was observed during

current injection through some of the channels (around 30%) at 6 kHz without applied stimulation.

4. Discussion

We have for the first time demonstrated the feasibility of using EIT to record spatially selective functional fascicles in a peripheral nerve. We were able to identify optimal recording parameters, and demonstrated the recording of physiologically relevant single channel impedance changes significantly related to the CAP propagating in the sciatic nerve. These had a SNR of 8 at the optimum recording frequency of approximately 6 kHz. The optimal current level for acquiring EIT signals was 30–50 μA (5–8 nC/phase) which was subthreshold and did not modify the action potential. The impedance signal in myelinated nerve was attributable to fast myelinated (A-beta/delta) sensory/motor afferent fibres conducting at 20–60 m s^{-1} [46]. There were no significant impedance changes (with $P < 0.05$) with slower and wider duration; this may have been due to the stimulation parameters as slower fibres require a wider stimulation pulse in order to activate or greater dispersion.

For the first time, we produced spatially distinguishable EIT images of fascicle specific impedance changes which corresponded to the known co-registered histomorphometric positions of the tibial and common peroneal fascicles. Although there were visible deviations on the single topographic distribution of the fascicles between EIT and histology (probably due to deformation caused during slice preparation), the average centre-to-centre mismatch error was below 100 μm .

4.1. Comparison of EIT and ISA

The instantaneous SNR in this work was 0.8 (−4 dB) at best, in comparison to 10 (20 dB) for simultaneous ISA implemented in this work, and real-time SNR of 2.5 (8 dB) reported in the published literature [36]. It is therefore clear that the SNR in ISA is greater; as a result, it was necessary to average for 7 min to improve this and also to yield the additional number of independent measurements required for EIT.

When applied to averaged data, both methods had a similar average mismatch error of <140 μm . However, it is visually apparent that image quality and resolution for EIT is superior to that for ISA. In one rat (figure 6, rat 3), ISA almost failed to reconstruct activity in the common peroneal fascicle as a single region, probably due to the contact impedance mismatch to which the method is very sensitive. Overall the accuracy of the fascicular prediction with EIT was 100% in comparison to 90% in case of simultaneous ISA, and 70%–80% with the method implemented in freely moving animals [36].

4.2. Study limitations and future work

The main limitation of the technique, as it is presented, is the poor SNR in comparison to ISA. Sufficient averaging is required in order to obtain reliable signals, so it is impossible

to apply the technique as it is in real time. In addition, if the data is to be recorded during spontaneous activity, dispersion of the CAP and partial volume effects may reduce this significantly further.

The present study reports the first use of this technique as a proof of concept for imaging fascicle-level activity. In principle, it is not limited, however, to only fascicle-level, and given enough electrodes around the nerve, it may be possible to improve the resolution further. In the future, we plan to use 32-electrode arrays where a theoretical resolution of <30 μm could be achieved. At present, a principal intended target is for imaging and selective stimulation in the human vagus nerve. This has a diameter of 3–4 mm and has about 30 fascicles. With the current resolution, this should permit identification of most fascicles although probably not sub-fascicular activity. However, this would still be superior to other existing methods.

EIT may be a powerful technique for determining the functional anatomy of fascicles in Electroceuticals, where the need for triggered repeated activation of a distal end-organ of interest is practicable. Although it would not currently be suitable for real-time motor control in neuroprosthetics, it may be possible to improve the SNR and temporal resolution of fast neural EIT in the future with the following developments. EIT data can be acquired in phase and frequency division multiplexing mode, where each electrode combination is assigned simultaneously with a unique frequency and phase; this allows parallel recording of all possible combinations [41]. SNR could be improved through spatiotemporal methods of activity extraction, for example, velocity-selective [47], or variance-based methods, similar to the ones used for advanced ISA algorithms [35]. In conclusion, ISA and fast neural EIT with neural cuffs represent complementary ways to provide localised fascicle information which is likely to be of significant benefit for neuroprosthetics and Electroceuticals. This work is the first presentation of this application; further advances may lead to improved temporal and spatial resolution. At present, EIT appears to offer improved spatial resolution which could be of value where averaging over tens of seconds or minutes is practical.

Acknowledgments

This research was supported by GSK-UCL collaboration grant ‘Imaging and selective stimulation of autonomic nerve traffic using EIT and a non-penetrating nerve cuff’, and EPSRC grant EP/M506448/1.

Authors would like to thank Professor Nick Donaldson and Implantable Devices Group (IDG) at UCL for providing the clean room for electrodes manufacturing. Authors also would like to thank Dr Christopher Chapman for helpful discussions during paper preparation.

Author contributions

KA and DH designed the experiments; JA provided engineering support and designed pieces of the hardware

equipment; CB and SH assisted with surgery and neural dissection; KA and MD performed the experiments and acquired the data; KA analysed the data. KA and DH interpreted the data. KA wrote the paper.

ORCID iDs

Kirill Aristovich  <https://orcid.org/0000-0002-2924-5680>

James Avery  <https://orcid.org/0000-0002-4015-1802>

Sana Hannan  <https://orcid.org/0000-0003-2241-8312>

References

- [1] Nicolelis M A L, Dimitrov D, Carmena J M, Crist R, Lehe G, Kralik J D and Wise S P 2003 Chronic, multisite, multielectrode recordings in macaque monkeys *Proc. Natl Acad. Sci. USA* **100** 11041–6
- [2] Bensmaia S J 2015 Biological and bionic hands : natural neural coding and artificial perception *Philos. Trans. R. Soc. B* **370** 20140209
- [3] Sunderland S 1945 The intraneural topography of the radial, median and ulnar nerves *Brain* **68** 243–99
- [4] Sunderland S and Ray L J 1948 The intraneural topography of the sciatic nerve and its potential divisions in man 1 BY *Brain* **71** 242–73
- [5] Lanciego J L and Wouterlood F G 2011 A half century of experimental neuroanatomical tracing *J. Chem. Neuroanat.* **42** 157–83
- [6] Sun K, Zhang J, Chen T, Chen Z, Li Z, Li H and Hu P 2009 Three-dimensional reconstruction and visualization of the median nerve from serial tissue sections *Microsurgery* **29** 573–7
- [7] Mathews K S, Wark H A C and Normann R A 2014 Assessment of rat sciatic nerve function following acute implantation of high density Utah slanted electrode array (25 electrodes mm⁻²) based on neural recordings and evoked muscle activity *Muscle Nerve* **50** 417–24
- [8] Davis T S, Wark H A C, Hutchinson D T, Warren D J, O'Neill K, Scheinblum T, Clark G A, Normann R A and Greger B 2016 Restoring motor control and sensory feedback in people with upper extremity amputations using arrays of 96 microelectrodes implanted in the median and ulnar nerves *J. Neural Eng.* **13** 36001
- [9] Tyler D J 2015 Neural interfaces for somatosensory feedback: bringing life to a prosthesis *Curr. Opin. Neurol.* **28** 574–81
- [10] Li L-J, Zhang J, Zhang F, Lineaweaver W C, Chen T-Y and Chen Z-W 2005 Longitudinal intrafascicular electrodes in collection and analysis of sensory signals of the peripheral nerve in a feline model *Microsurgery* **25** 561–5
- [11] Wark H A C, Mathews K S, Normann R A and Fernandez E 2014 Behavioral and cellular consequences of high-electrode count Utah arrays chronically implanted in rat sciatic nerve *J. Neural Eng.* **11** 46027
- [12] Christensen M B, Wark H A C and Hutchinson D T 2016 A histological analysis of human median and ulnar nerves following implantation of Utah slanted electrode arrays *Biomaterials* **77** 235–42
- [13] Raspopovic S et al 2014 Restoring natural sensory feedback in real-time bidirectional hand prostheses *Sci. Transl. Med.* **6** 222ra19
- [14] Clark G A, Ledbetter N M, Warren D J and Harrison R R 2011 Recording sensory and motor information from peripheral nerves with Utah slanted electrode arrays *Conf. Proc. ... Annual Int. Conf. IEEE Eng. Med. Biol. Soc.* vol 2011 pp 4641–4
- [15] Sharma V, McCreery D B, Han M and Pikov V 2010 Bidirectional telemetry controller for neuroprosthetic devices *IEEE Trans. Neural Syst. Rehabil. Eng.* **18** 67–74
- [16] Chakravarthy K, Nava A, Christo P J and Williams K 2016 Review of recent advances in peripheral nerve stimulation (PNS) *Curr. Pain Headache Rep.* **20** 60
- [17] Navarro X, Krueger T B, Lago N, Micera S, Stieglitz T and Dario P 2005 A critical review of interfaces with the peripheral nervous system for the control of neuroprostheses and hybrid bionic systems *J. Peripher. Nerv. Syst.* **10** 229–58
- [18] Witkowska-Wrobel A, Aristovich K, Faulkner M, Avery J and Holder D 2018 Feasibility of imaging epileptic seizure onset with EIT and depth electrodes *NeuroImage* **173** 311–21
- [19] Somersalo E, Cheney M and Isaacson D 1992 Existence and uniqueness for electrode models for electric current computed tomography *SIAM J. Appl. Math.* **52** 1023–40
- [20] Isaacson D 1986 Distinguishability of conductivities by electric current computed tomography *IEEE Trans. Med. Imaging* **5** 91–5
- [21] Cole K S and Curtis H J 1939 Electric impedance of the squid giant axon during activity *J. Gen. Physiol.* **22** 649–70
- [22] Holder D S 1992 Impedance changes during the compound nerve action potential: implications for impedance imaging of neuronal depolarisation in the brain *Med. Biol. Eng. Comput.* **30** 140–6
- [23] Liston A, Bayford R and Holder D 2012 A cable theory based biophysical model of resistance change in crab peripheral nerve and human cerebral cortex during neuronal depolarisation: implications for electrical impedance tomography of fast neural activity in the brain *Med. Biol. Eng. Comput.* **50** 425–37
- [24] Aristovich K Y, Dos Santos G S and Holder D S 2015 Investigation of potential artefactual changes in measurements of impedance changes during evoked activity: implications to electrical impedance tomography of brain function *Physiol. Meas.* **36** 1245–59
- [25] Oh T, Gilad O, Ghosh A, Schuettler M and Holder D S 2011 A novel method for recording neuronal depolarization with recording at 125–825 Hz: implications for imaging fast neural activity in the brain with electrical impedance tomography *Med. Biol. Eng. Comput.* **49** 593–604
- [26] Aristovich K, Packham B, Koo H, Dos Santos G S, McEvoy A and Holder D 2016 Imaging fast electrical activity in the brain with electrical impedance tomography *NeuroImage* **124** 204–13
- [27] Vongerichten A N, Santos G S D, Aristovich K, Avery J, McEvoy A, Walker M and Holder D S 2016 Characterisation and imaging of cortical impedance changes during interictal and ictal activity in the anaesthetised rat *NeuroImage* **124** 813–23
- [28] Badia J, Pascual-Font A, Vivó M, Udina E and Navarro X 2010 Topographical distribution of motor fascicles in the sciatic-tibial nerve of the rat *Muscle Nerve* **42** 192–201
- [29] Bäumer P, Weiler M, Bendszus M and Pham M 2015 Somatotopic fascicular organization of the human sciatic nerve demonstrated by MR neurography *Neurology* **84** 1782–7
- [30] Zariffa J 2014 A review of source separation and source localization approaches in peripheral nerves 2014 48th *Asilomar Conf. on Signals, Systems and Computers* (IEEE) pp 293–8
- [31] Grech R, Cassar T, Muscat J, Camilleri K P, Fabri S G, Zervakis M, Xanthopoulos P, Sakkalis V and Vanrumste B 2008 Review on solving the inverse problem in EEG source analysis *J. Neuroeng. Rehabil.* **5** 25

- [32] Buzsáki G, Anastassiou C A and Koch C 2012 The origin of extracellular fields and currents—EEG, ECoG, LFP and spikes *Nat. Rev. Neurosci.* **13** 407–20
- [33] Zariffa J, Nagai M K, Schuettler M, Stieglitz T, Daskalakis Z J and Popovic M R 2011 Use of an experimentally derived leadfield in the peripheral nerve pathway discrimination problem *IEEE Trans. Neural Syst. Rehabil. Eng.* **19** 147–56
- [34] Dweiri Y M, Stone M A, Tyler D J, McCallum G A and Durand D M 2016 Fabrication of high contact-density, flat-interface nerve electrodes for recording and stimulation applications *J. Vis. Exp.* **116** e54388
- [35] Eggers T E, Dweiri Y M, McCallum G A and Durand D M 2017 Model-based Bayesian signal extraction algorithm for peripheral nerves *J. Neural Eng.* **14** 56009
- [36] Dweiri Y M, Eggers T E, Gonzalez-Reyes L E, Drain J, McCallum G A and Durand D M 2017 Stable detection of movement intent from peripheral nerves: chronic study in dogs *Proc. IEEE* **105** 50–65
- [37] Wodlinger B and Durand D M 2009 Localization and recovery of peripheral neural sources with beamforming algorithms *IEEE Trans. Neural Syst. Rehabil. Eng.* **17** 461–8
- [38] Wodlinger B and Durand D M 2011 Selective recovery of fascicular activity in peripheral nerves *J. Neural Eng.* **8** 56005
- [39] Ventouras E, Papageorgiou C, Uzunoglu N, Koulouridis S, Rabavilas A and Stefanis C 2000 Tikhonov regularization techniques in simulated brain electrical tomography *Biotechnol. Biotechnol. Equip.* **14** 95–9
- [40] Vongerichten A, Aristovich K, dos Santos G S, McEvoy A W and Holder D S 2014 Design for a three-dimensional printed laryngoscope blade for the intubation of rats *Lab Anim.* **43** 140–2
- [41] Avery J, Dowrick T, Faulkner M, Goren N and Holder D 2017 A versatile and reproducible multi-frequency electrical impedance tomography system *Sensors* **17** 280
- [42] Kao T-J, Newell J C, Saulnier G J and Isaacson D 2003 Distinguishability of inhomogeneities using planar electrode arrays and different patterns of applied excitation *Physiol. Meas.* **24** 403–11
- [43] Aristovich K Y, Santos G S D, Packham B C and Holder D S 2014 A method for reconstructing tomographic images of evoked neural activity with electrical impedance tomography using intracranial planar arrays *Physiol. Meas.* **35** 1095–109
- [44] Jehl M, Dedner A, Betcke T, Aristovich K, Kloforn R and Holder D 2014 A fast parallel solver for the forward problem in electrical impedance tomography *IEEE Trans. Biomed. Eng.* **62** 126–37
- [45] Vallaghé S, Papadopoulou T and Clerc M 2009 The adjoint method for general EEG and MEG sensor-based lead field equations *Phys. Med. Biol.* **54** 135–47
- [46] Gasser H S 1941 The classification of nerve fibers *Ohio J. Sci.* **41** 3–145
- [47] Metcalfe B W, Nielsen T N, de Donaldson N N, Hunter A J and Taylor J T 2018 First demonstration of velocity selective recording from the pig vagus using a nerve cuff shows respiration afferents *Biomed. Eng. Lett.* **8** 127–36